Time-Resolved Digital Data Processing Enhancements in Neutron Active Interrogation

Colton Graham[1], Junwoo Bae[1], Christopher Meert[1], Abbas Jinia[1], Oskar Searfus[1], Shaun Clarke[1], Sara Pozzi[1], and Igor Jovanovic[1]

[1]Department of Nuclear Engineering and Radiological Sciences, University of Michigan, 2355 Bonisteel Blvd, Ann Arbor, MI 48109, United States

May 12, 2023

Abstract

Detecting shielded contraband material, including illicit drugs, explosives, and special nuclear material using nuclear techniques has been a persistent technical challenge. The signatures from contraband materials are often relatively weak and poorly separated from the background, requiring the use of long measurement times and high radiation doses from the interrogating source. We are exploring new digital pulse processing techniques for active neutron interrogation to enhance the detection of concealed contraband and special nuclear material with a focus on prompt gamma-ray signatures for drug and explosive detection and fast neutron detection for special nuclear material. The new detection systems make use of digital data acquisition from inorganic and organic scintillators along with the time structure of deuterium-deuterium and deuterium-tritium fast neutron generator interrogation sources to improve the signal-to-noise ratio of the measurements. The detection system additionally makes use of a reconfigurable water-based collimation system to reduce the production of activation gamma rays in the environment and to shield the detectors from fast and thermal internal neutron activation. We characterized the fast neutron time profile of the Thermo Scientific P211 DT neutron generator using organic scintillators and a gamma-blind He-4 recoil-based fast neutron detector. We discuss the spectral and time profiles resulting from active interrogation measurements performed with various contraband simulants and a range of inorganic scintillators, including fast inorganic scintillators such as $LaBr_3$. We additionally discuss maximum likelihood estimation maximization-based spectral reconstruction techniques in conjunction with detecting prompt gamma rays with organic scintillators. We show the detection of prompt inelastic gamma-ray signatures from carbon- and nitrogen-rich objects that may allow for the measurement of sample stoichiometry to distinguish explosive and narcotic contraband from benign samples. Based on these methods, combined spectro-temporal analysis is being developed for detecting shielded contraband with improved sensitivity.

1 Introduction

Concealed contraband (*e.g.*, explosives, narcotics, and special nuclear material) can be detected through fast neutron activation. For explosives and narcotics, neutron capture and neutron inelastic scattering gamma rays produced by hydrogen, carbon, nitrogen, and oxygen (HCNO) are

the potential observables [1, 2, 3, 4, 5]. The relative abundance of gamma rays associated with these elements can give insight into the stoichiometry of the activation target, which can allow for discrimination of contraband from benign objects [2, 6, 7]. Special nuclear material (SNM) can be detected through both neutron and gamma-ray signals emitted under fast neutron interrogation [8, 9]. However, active interrogation systems are yet to be widely deployed at security checkpoints because the systems are complicated to develop and use, can deliver a substantial radiation dose to operators, and are not cost-effective. The current systems also do not offer sufficient efficiency and specificity to detect activation signals that are weak compared to the interrogating signal, which makes the measurement times prohibitively long.

Digital pulse analysis can increase the sensitivity of gamma-ray and neutron detection for active interrogation applications. Pileup correction and reconstruction can be used to improve sensitivity in the high-flux environment of an interrogating source [10]. In some instances, time gating of gamma-ray signals relative to the timing structure of the interrogating source can be used to improve the signal-to-background ratio [11]. We have been working to demonstrate improvement in the sensitivity and practicality of active interrogation detection systems using digital techniques. For example, we discuss digital spectral reconstruction to make use of organic scintillators for gamma-ray spectroscopy in the active interrogation setting.

2 Measurement of DT Neutron Time Profile

The time profile of pulsed DT neutrons determines the timing of gamma rays produced through fast neutron activation. Thus, measurement of the 14.1-MeV neutrons' time profile can allow for the isolation of different gamma rays of interest. For example, gamma rays produced through inelastic neutron scattering occur in approximate coincidence with the emission of neutrons from the probing generator, while gamma rays produced in neutron capture are delayed by the neutron thermalization time, which is needed for capture to take place with high probability. The DT neutron generator used for our measurements is the P211 by Thermo Scientific [12]. To measure the neutron time profile, several fast nuclear recoil-based detectors were used. Trans-stilbene [13] and organic glass scintillator (OGS) [14] solid-state scintillators were used alongside an EJ-309 liquid organic scintillator [15]. Pulse-shape discrimination (PSD) was used to separate the neutron signal from the abundant gamma rays and X rays. The time profile was also measured with a pressurized ^{4}He gas detector that operates on the principle of scintillation induced by ^{4}He recoils in neutron elastic scattering. Such a detector is advantageous for this measurement due to its intrinsic low gamma-ray sensitivity [16], preventing interference of activation gamma rays with neutrons and reducing pileup. In each case, a light output threshold was set to isolate the 14.1-MeV neutrons directly incident from the neutron generator and reject neutrons that scatter in the environment and then interact with the detectors. Neutrons that undergo scattering generally transfer a significant fraction of their kinetic energy and thus can be rejected by setting a light output threshold. These neutrons are undesirable as the time to scatter can broaden the measured time profile. For comparison with the neutron time profile, the time profile of activation gamma rays was also measured with a $LaBr_3$ detector, which is a fast inorganic scintillator [17]. Data were collected from each detector as digital traces using various CAEN digitizers. Also collected was the timing signal from the DT generator's pulse-forming network, referred to as the DT trigger, which acts as a time tag for the neutron emission from the generator. Data were analyzed both during measurement using the CAEN CoMPASS software [18] and offline using the ROOT data analysis framework [19]. The timing relative to the most recent DT trigger of each event was then

histogrammed and is shown in Figure 1 for each detector.

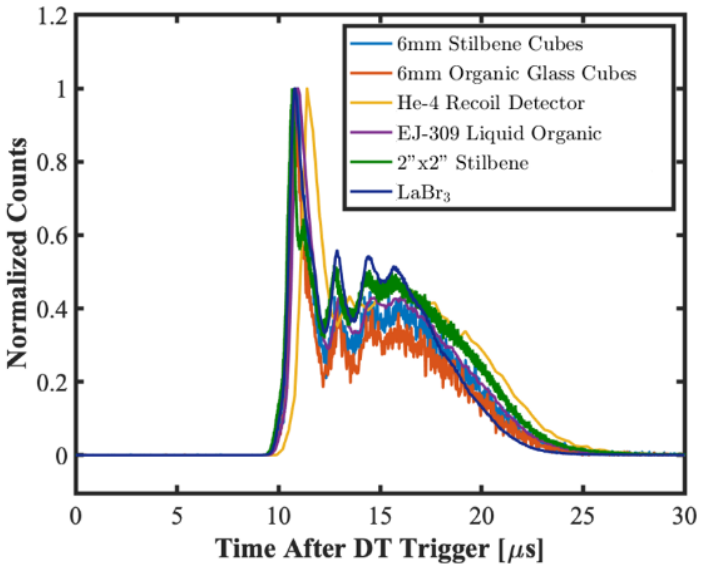

Figure 1: Measured time profile of 14.1 MeV neutrons from P211 DT generator

The time profile has a width of 15–20 µs and a clear initial peak with a width of 1 µs. This fast initial peak is advantageous as many prompt gamma rays are produced during this time period, while relatively few neutrons will have been thermalized and captured, resulting in the minimal background from neutron capture gamma rays. There is a reasonable agreement in the shape of the DT neutron profile measured by different detection methods, providing some confidence in the accuracy of the measured time profile. The gamma-ray time profile measured with the $LaBr_3$ detector follows the measured time profile of fast neutrons from the neutron generator, confirming that the gamma-ray signals seen originate primarily from the DT neutron activation.

3 Fast Neutron Activation Measurements

3.1 Collimation of DT Neutrons

Fast neutron collimation is advantageous for prompt gamma-ray neutron activation analysis. Fast and thermal neutron activation can induce long-lived backgrounds in many inorganic scintillators [20, 21]. The interrogating neutrons can also act as a background term for the measurement of activation neutrons. This background can be reduced by fast neutron shielding to collimate the fast neutron source to a beam. Additionally, by collimating fast neutrons, background activation in the environment can be localized to angles subtended by the collimated beam. This reduces the amount of gamma-ray shielding needed to reduce activation background by decreasing the area over which that background is produced. A fast neutron collimator made from plastic bricks filled with water was designed and constructed and can be seen in Figure 2a. Water is attractive for fast neutron shielding due to the high hydrogen content which allows for thermalization of fast neutrons. Discrete water bricks can be easily reconfigured based on the desired geometry for a given measurement. To optimize the collimation design, the fast neutron and gamma-ray profile was simulated using MCNP6 [22]. Based on the simulation, a uniform collimator with a thickness

of approximately 1 meter is optimal to collimate neutrons while still allowing high neutron flux to reach activation targets. Measurements with liquid organic scintillators revealed an approximate order of magnitude reduction in fast neutron flux from the beam center to being outside of the beam profile. Activation measurements were conducted in the configuration shown in Figure 2b such that the activation targets were placed in the path of the uncollimated fast neutron beam, while gamma-ray detectors were placed outside of the beam path. Several inches of lead and other high-Z gamma-ray shielding were placed around the gamma-ray detectors to minimize the background from fast neutron activation in the environment. In particular, shielding is placed between the collimator and the detectors due to the large background from neutron thermalization and capture within the collimator.

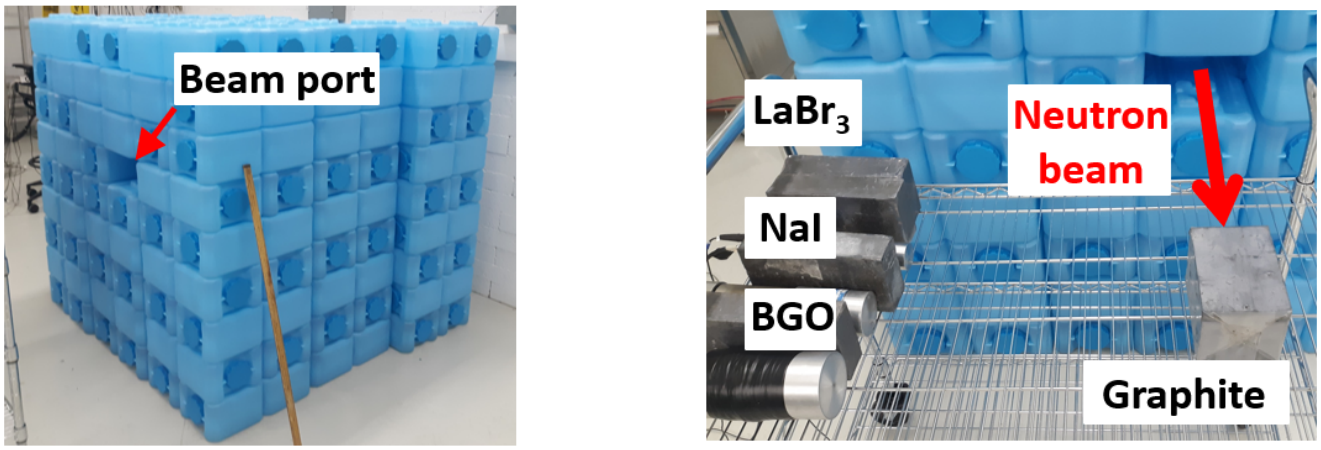

(a) Water based collimation system

(b) Example measurement configuration with a graphite activation target

Figure 2: Fast neutron collimation system for activation measurements

3.2 Time-Correlated Gamma Ray Spectroscopy

The measured normalized energy deposition spectrum from a $LaBr_3$ detector and a graphite activation target is shown in Figure 3a. This spectrum is shown for three separate time gates: all events, prompt events, and delayed events. The prompt time region refers to the time frames during which the DT generator produces neutrons, while the delayed region refers to a 20 µs window immediately after the DT generator stops producing neutrons. The prompt spectrum is harder due to the average energy of inelastic neutron scattering gamma rays being relatively high. In contrast, the delayed spectrum shows a more prominent photopeak and Compton scattering signature of the 2.2-MeV gamma ray from thermal neutron capture on hydrogen. This time dependence of the spectrum is due to the delay caused by the time for fast neutrons to thermalize and capture. This suggests that the signal-to-background ratio for detecting prompt and delayed gamma rays can be increased by appropriately selecting different periods of time relative to the neutron generator pulse. Despite this, there is no clear spectral signature of a 4.4-MeV gamma ray from inelastic neutron scattering on ^{12}C. This may be due to high pileup during measurement, which particularly impacts the gamma-ray signals created during the neutron pulse.

The time-spectral correlation is confirmed by observing the time profile of different spectral regions as shown in Figure 3b. As expected, the events comprising the photopeak of the 2.2-MeV gamma

ray from H(n,γ) make a greater relative contribution to the count rate after the neutron pulse from the generator terminates, while the events in the 4–5 MeV region, selected to encompass the photopeak of the carbon inelastic scattering gamma rays, make a greater relative contribution to the signal during the neutron pulse.

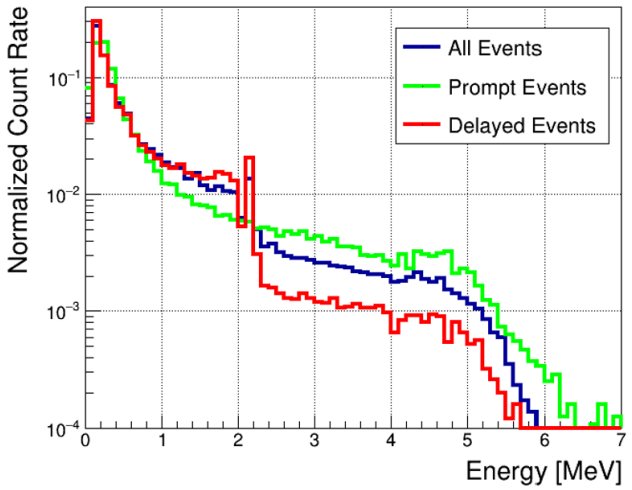

(a) Time correlated graphite activation spectrum measured with $LaBr_3$

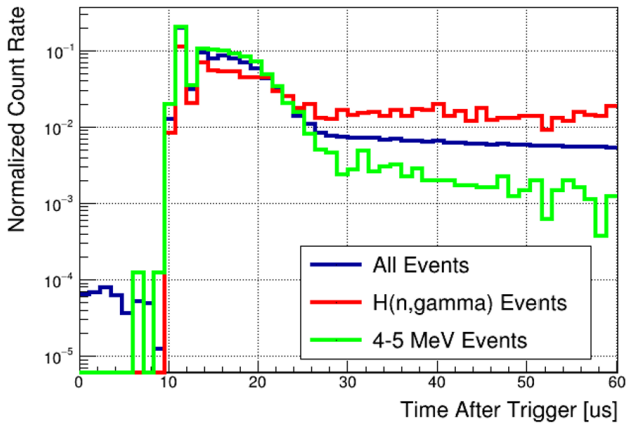

(b) Time profile for various activation spectral regions

Figure 3: Time and spectral correlation from $LaBr_3$ activation measurement

4 Organic Scintillators in Fast Neutron Activation Measurements

Despite their low average atomic number, organic scintillators are attractive for prompt gamma-ray neutron activation analysis because their fast response time makes them relatively resistant to pileup in high-flux environments [23]. They additionally do not suffer from the long-lived fast neutron activation present in many inorganic scintillators. They are cheap and easily scalable, allowing for the construction of cost-efficient and sensitive detection systems. However, gamma rays primarily interact in organic scintillators by Compton scattering. This is disadvantageous as compared to higher-Z inorganic scintillators, where photopeaks can be observed, allowing for relatively easy identification of gamma-ray signals of interest. The primary identifying feature for different gamma rays in organic scintillators is the Compton edge. However, using the Compton edge to identify individual gamma rays is generally more complicated.

4.1 MLEM Recoil Spectrum Reconstruction

To identify signatures of interest from the measured light output spectrum, maximum likelihood expectation maximization (MLEM) can be used. MLEM uses an iterative solution from the measured light output spectrum to reconstruct the incident energy spectrum:

$$\mathbf{s} = \mathbf{R}\mathbf{x} \Rightarrow x_j^{(k+1)} = \frac{x_j^k}{\sum_i R_{ij}} \sum_i R_{ij} \frac{s_i}{\sum_l R_{il} x_l^{(k)}}, \tag{4.1}$$

where **s** is the discretized measured light output spectrum, **R** is the response matrix of the detector that converts the gamma ray energy to light output, and **x** is the underlying incident energy spectrum that needs to be reconstructed [24, 25]. Spectral reconstruction allows for the identification of signatures of interest by selecting simple peaks known to correspond to elements or isotopes of interest.

The response matrix was generated through simulation in the Geant4 framework [26, 27, 28] and through measurement of the detector energy resolution. The energy deposition spectrum was simulated for incident gamma rays with energies up to 12 MeV in 0.05-MeV bins. A simplified geometry consisting of only the detector and source was used in the simulation, neglecting the impact of measurement geometry on the response matrix. The source geometry is generally not known *a priori*, and thus neglecting the source geometry allows for standardization of the spectral reconstruction. Incorporating measurement geometry into the detector response model is one potential future improvement for this spectral reconstruction method. The simulated energy deposition spectra are then converted to light output spectra assuming Gaussian broadening according to the measured energy resolution. The energy resolution is determined by fitting the simulated energy deposition spectrum with the measured recoil spectrum from gamma-ray check sources. Fitting is based on a five-parameter space corresponding to two parameters of linear calibration between pulse integral and light output and three parameters of energy resolution as a function of light output:

$$\frac{\Delta E}{E} = \sqrt{\alpha^2 + \frac{\beta^2}{E} + \frac{\gamma^2}{E^2}}, \tag{4.2}$$

where α, β, and γ are the fitting parameters, and E is the light output [29]. A genetic algorithm is used to sweep this broad parameter space where the quality of fit is checked with a χ^2 test at the Compton edge. An example of this fitting for ^{137}Cs is shown in Figure 4. The Compton edge is selected for fitting as the spectrum beyond the compton edge is relatively flat, which does not allow for the resolution parameters to be clearly defined.

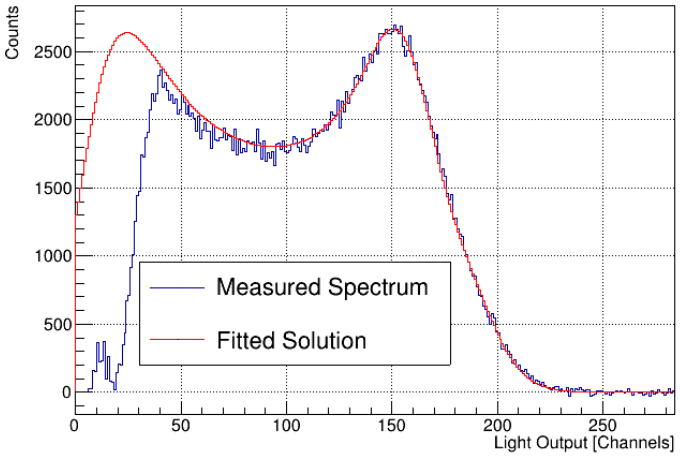

Figure 4: Example of fitting of simulated ^{137}Cs light output spectrum to measured spectrum at Compton edge with a genetic algorithm

This fitting was performed for ^{137}Cs, ^{22}Na, and ^{60}Co gamma-ray check sources. The energy resolution at the Compton edge energy from fitting is selected for each Compton edge and then collectively fitted to the energy resolution function, Equation (4.2). The results of this fitting are

shown in Figure 5. The fitted energy resolution function is used in preparing the response matrix by broadening the simulated energy deposition spectra.

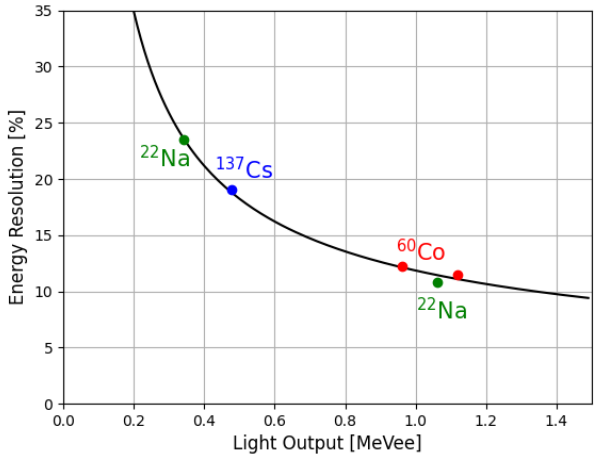

Figure 5: Fitted resolution function for liquid organic scintillator

As an example of MLEM spectral reconstruction, the measured light output spectrum and corresponding reconstructed spectrum from a measurement with a ^{152}Eu gamma-ray check source is shown in figure 6. ^{152}Eu has a relatively complex gamma-ray emission spectrum. The most prominent gamma-ray energies are additionally labelled with dashed lines in figure 6. The MLEM reconstructed spectrum exhibits clear peaks at nearly all of the major gamma ray energies and exhibits only spurious peaks at other energies, demonstrating accurate spectral reconstruction.

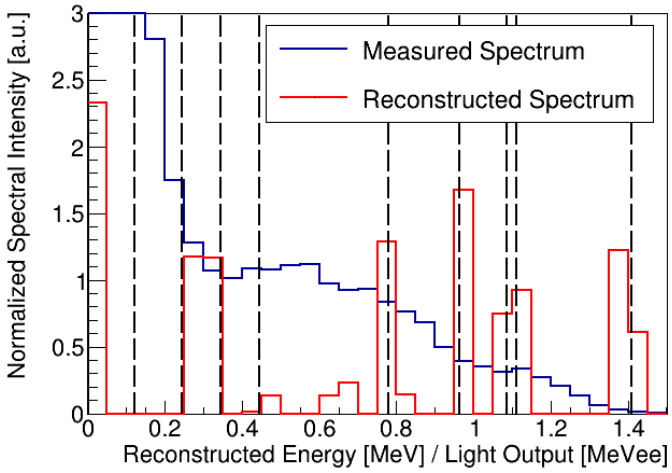

Figure 6: Example spectral reconstruction for ^{152}Eu gamma-ray source with measured light output. Most prominent gamma-ray energies are labeled with dashed lines.

4.2 Application to Fast Neutron Activation

Measurements of gamma-ray signatures of interest with organic scintillators were conducted in the same manner as with inorganic scintillators using the P211 DT neutron generator and water-based collimator. A 4" × 6" volume of deuterated liquid organic scintillator (EJ-315, Eljen)

was used for measurement. Deuterated organic scintillators are attractive in this context due to the higher nuclear recoil quenching associated with deuterons over proton recoils [29], which decreases the electron-equivalent light output for nuclear recoils. Because of quenching and the collimation of fast neutrons, there are relatively few neutron pulses in the spectral region of interest for prompt gamma rays, which is generally above 4 MeV. Thus, the impact of neutrons on the measured light output spectrum can be neglected without the need for pulse-shape discrimination. By not integrating the signal long enough to allow for pulse-shape discrimination, the rate of pulse pileup can be drastically reduced, allowing for easier detection of prompt gamma-ray signals. Such spectral reconstruction could also be done with non-deuterated organic scintillators. For comparison, the graphite activation reconstructed spectrum from the gamma-ray and neutron contributions is shown in Figure 7b along with the total reconstructed spectrum. The pulse-shape discrimination fiducial cuts used to identify neutrons and gamma rays are shown in Figure 7a. The neutron contribution to the signal that distinguishes the gamma-ray only and gamma ray - neutron combined reconstructed spectra is minimal, confirming that there are few neutrons that need to be rejected through pulse-shape discrimination in this case.

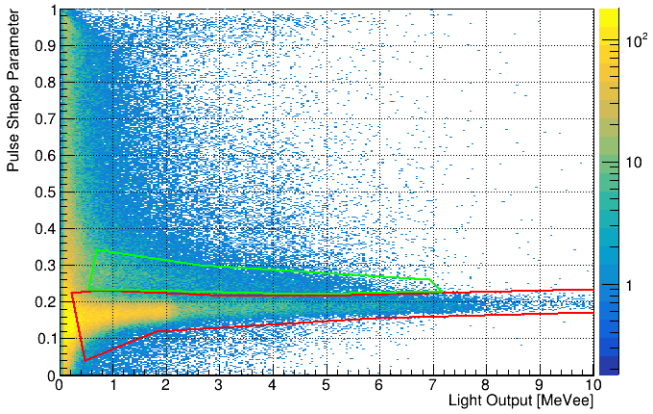

(a) Fiducial cuts used to identify neutron and gamma-ray events for comparison of neutron contribution

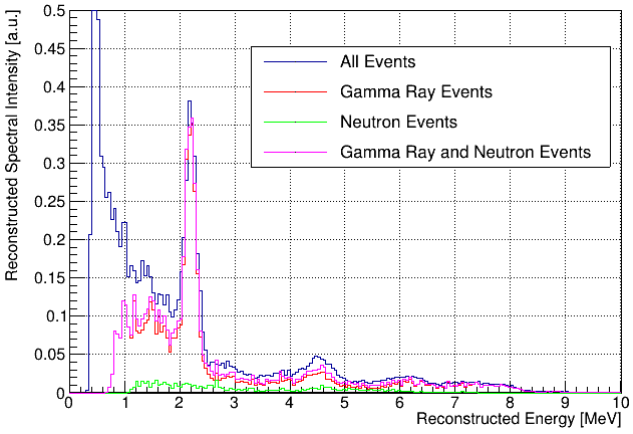

(b) MLEM reconstructed spectrum from gamma-ray and neutron contribution.

Figure 7: Comparison of neutron and gamma-ray contributions to spectrum with EJ-315 deuterated liquid organic scintillator

Measurements were conducted with a carbon-rich graphite target and a nitrogen-rich melamine ($C_3H_6N_6$) target. The active background was also measured to subtract from the activation target measurements. Initial spectral reconstruction was performed with the graphite target data due to the relative simplicity of the response from neutron inelastic scattering on ^{12}C, which has only one prominent gamma-ray energy at 4.4 MeV. To determine the impact of time gating on the spectral reconstruction, the measured light output spectrum was gated according to all measured events; all prompt events, *i.e.*, the events measured when the DT neutron generator produces neutrons (10–25 µs on the scale shown in Figure 1); all prompt peak events, *i.e.*, during the initial spike of the DT neutron profile; and delayed events, after the DT neutron generator stops producing neutrons (greater than 30 µs as shown in Figure 1). The reconstructed gamma-ray spectrum for each time gate is shown in Figure 8 along with the time corresponding time gates.

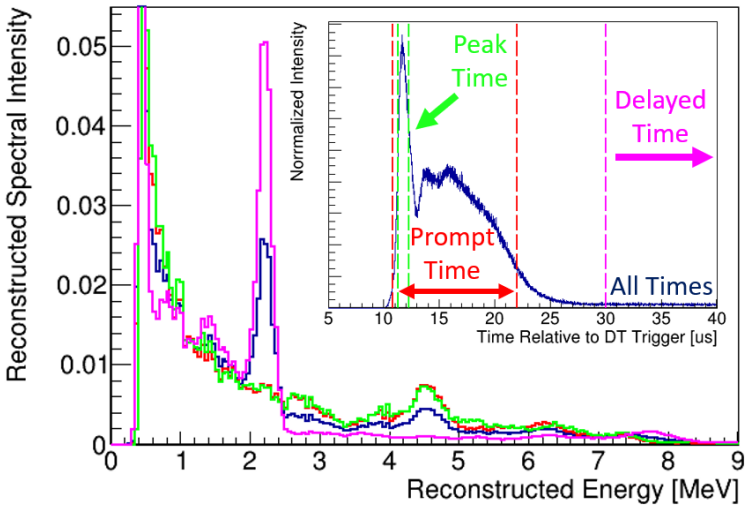

Figure 8: Reconstructed graphite activation spectrum with various time gates

Both the reconstructed gamma-ray spectrum of all prompt events and the spectrum of only the peak prompt events show similar shapes but exhibit a more prominent peak corresponding to the 4.4-MeV prompt gamma-ray from carbon neutron inelastic scatter than the spectrum incorporating all events. Note that the spectrum from delayed events exhibits no such peak, as expected from the absence of sufficiently energetic neutrons during the delayed time period. Based on this, a time gate corresponding to all prompt events, *i.e.*, all events when the DT neutron generator is on, is applied to isolate prompt events while maximizing sensitivity by allowing for the statistics to build up. The active background subtracted spectra measured from graphite and melamine activation targets while applying this time gate are shown in Figures 9a and 9b. The energies of the most intense anticipated prompt gamma rays are labeled.

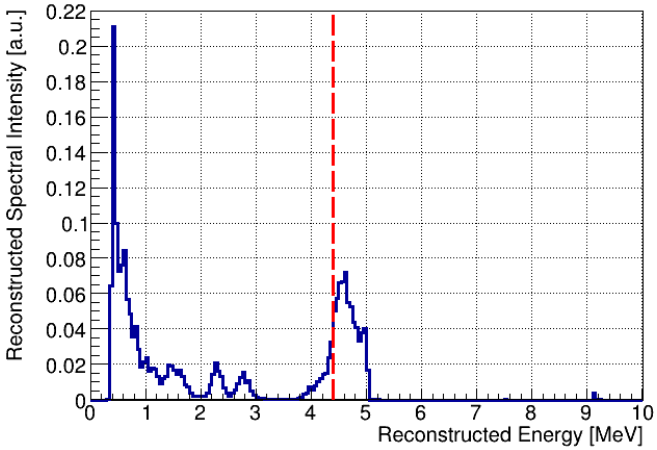

(a) Graphite spectrum. Major carbon inelastic neutron scattering gamma rays labeled in red

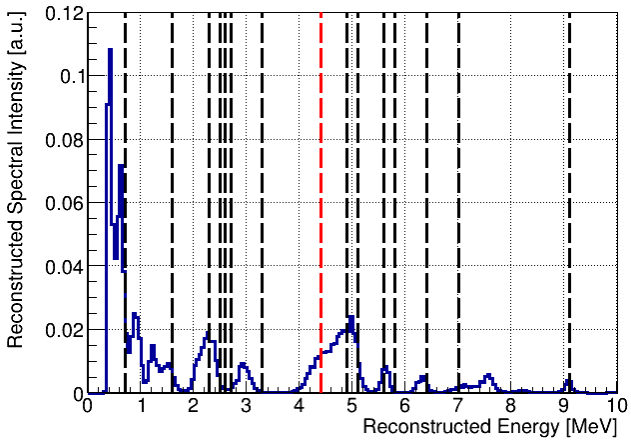

(b) Melamine spectrum. Major nitrogen inelastic recoil gamma rays are labeled as black lines, while major carbon inelastic recoil gamma rays are labeled as red lines

Figure 9: Active background subtracted MLEM reconstructed spectrum from graphite and melamine activation targets

The graphite active background subtracted spectrum shows a clear broad peak in the region of 4–5 MeV that corresponds to the prompt gamma ray of interest. The cause of the asymmetric broadening of this peak is unclear but may be due to interference from a prominent 4.9-MeV gamma ray from thermal neutron capture by ^{12}C. The reconstructed spectrum from melamine activation is more complex but displays many of the prompt gamma ray lines expected from neutron inelastic scattering on ^{14}N. In particular, the prominent 5.1-MeV gamma-ray line can be clearly seen despite the overlap with the 4.4-MeV carbon line.

5 Conclusion

We discussed the use of digital analysis and time gating for improvement of detection of explosives, contraband, and special nuclear material via detection of fast neutron activation gamma rays. In particular, the time profile of pulsed DT neutrons is measured and applied in gamma-ray spectroscopy with inorganic and organic scintillators. This time profile allows for time gating to improve the signal-to-background ratio of particular spectral regions of interest. We additionally discussed MLEM-based spectral reconstruction for the detection of prompt gamma rays in organic scintillators. We show successful detection of carbon and nitrogen prompt neutron inelastic scattering gamma rays with this method. It may be possible to perform crude activation sample stoichiometry of carbon and nitrogen content based on the reconstruction results. In combination with detection of neutron capture signal from hydrogen and oxygen, it may be possible to detect and distinguish explosive and narcotic contraband. Further experiments need to be conducted with activation samples of varying content to show the impact of sample stoichiometry on the reconstructed gamma-ray spectrum.

6 Acknowledgements

This project was funded under DHS cooperative agreement number 21CWMDARI00040-01-00 and was partially supported by the Department of Energy National Nuclear Security Administration, Consortium for Monitoring, Verification and Technology (DE-NE000863) and the Department of Energy, Nuclear Energy University Program Fellowship.

References

[1] D. Brown and T. Gozani, "Cargo inspection system based on pulsed fast neutron analysis," *Nuclear Instruments and Methods in Physics Research Section B: Beam Interactions with Materials and Atoms*, vol. 99, no. 1, pp. 753–756, 1995, application of Accelerators in Research and Industry '94. [Online]. Available: https://www.sciencedirect.com/science/article/pii/0168583X94007497

[2] D. Strellis and T. Gozani, "Classifying threats with a 14-mev neutron interrogation system," *Applied Radiation and Isotopes*, vol. 63, no. 5, pp. 799–803, 2005, 8th International Conference on Applications of Nuclear Techniques. [Online]. Available: https://www.sciencedirect.com/science/article/pii/S0969804305001697

[3] T. Gozani, "Novel applications of fast neutron interrogation methods," *Nuclear Instruments and Methods in Physics Research Section A: Accelerators, Spectrometers, Detectors*

and Associated Equipment, vol. 353, no. 1, pp. 635–640, 1994. [Online]. Available: https://www.sciencedirect.com/science/article/pii/016890029491740X

[4] A. Buffler, "Contraband detection with fast neutrons," *Radiation Physics and Chemistry*, vol. 71, no. 3, pp. 853–861, 2004, 9th International Symposium on Radiation Physics (ISRP-9). [Online]. Available: https://www.sciencedirect.com/science/article/pii/S0969806X04003068

[5] Z. D. Whetstone and K. J. Kearfott, "A review of conventional explosives detection using active neutron interrogation," *Journal of Radioanalytical and Nuclear Chemistry*, vol. 301, no. 3, pp. 629–639, Sep 2014. [Online]. Available: https://doi.org/10.1007/s10967-014-3260-5

[6] A. Barzilov and I. Novikov, "Material classification by analysis of prompt photon spectra induced by 14-mev neutrons," *Physics Procedia*, vol. 66, pp. 396–402, 2015, the 23rd International Conference on the Application of Accelerators in Research and Industry - CAARI 2014. [Online]. Available: https://www.sciencedirect.com/science/article/pii/S1875389215002023

[7] P. Gokhale and E. Hussein, "A 252cf neutron transmission technique for bulk detection of explosives," *Applied Radiation and Isotopes*, vol. 48, no. 7, pp. 973–979, 1997. [Online]. Available: https://www.sciencedirect.com/science/article/pii/S0969804397000286

[8] D. Slaughter, M. Accatino, A. Bernstein, J. Candy, A. Dougan, J. Hall, A. Loshak, D. Manatt, A. Meyer, B. Pohl, S. Prussin, R. Walling, and D. Weirup, "Detection of special nuclear material in cargo containers using neutron interrogation." [Online]. Available: https://www.osti.gov/biblio/15005260

[9] K. Ogren, J. Nattress, and I. Jovanovic, "Discriminating uranium isotopes based on fission signatures induced by delayed neutrons," *Phys. Rev. Appl.*, vol. 14, p. 014033, Jul 2020. [Online]. Available: https://link.aps.org/doi/10.1103/PhysRevApplied.14.014033

[10] A. J. Jinia, T. E. Maurer, C. A. Meert, M. Y. Hua, S. D. Clarke, H.-S. Kim, D. D. Wentzloff, and S. A. Pozzi, "An artificial neural network system for photon-based active interrogation applications," *IEEE Access*, vol. 9, pp. 119 871–119 880, 2021.

[11] A. P. Barzilov, I. S. Novikov, and B. Cooper, "Computational study of pulsed neutron induced activation analysis of cargo," *Journal of Radioanalytical and Nuclear Chemistry*, vol. 282, no. 1, pp. 177–181, Oct 2009. [Online]. Available: https://doi.org/10.1007/s10967-009-0298-x

[12] *P 211 Neutron Generator*, Thermo Scientific, 2008. [Online]. Available: https://www.thermofisher.com/document-connect/document-connect.html?url=https://assets.thermofisher.com/TFS-Assets/CAD/Specification-Sheets/D10500 .pdf

[13] N. Zaitseva, A. Glenn, L. Carman, H. Paul Martinez, R. Hatarik, H. Klapper, and S. Payne, "Scintillation properties of solution-grown trans-stilbene single crystals," *Nuclear Instruments and Methods in Physics Research Section A: Accelerators, Spectrometers, Detectors and Associated Equipment*, vol. 789, pp. 8–15, 2015. [Online]. Available: https://www.sciencedirect.com/science/article/pii/S0168900215004635

[14] J. S. Carlson and P. L. Feng, "Melt-cast organic glasses as high-efficiency fast neutron scintillators," *Nuclear Instruments and Methods in Physics Research Section A: Accelerators, Spectrometers, Detectors and Associated Equipment*, vol. 832, pp. 152–157, 2016. [Online]. Available: https://www.sciencedirect.com/science/article/pii/S0168900216306866

[15] A. Kaplan, M. Flaska, A. Enqvist, J. Dolan, and S. Pozzi, "Ej-309 pulse shape discrimination performance with a high gamma-ray-to-neutron ratio and low threshold," *Nuclear Instruments and Methods in Physics Research Section A: Accelerators, Spectrometers, Detectors and Associated Equipment*, vol. 729, pp. 463–468, 2013. [Online]. Available: https://www.sciencedirect.com/science/article/pii/S016890021301108X

[16] O. Searfus, K. Ogren, and I. Jovanovic, "Digital pulse analysis for fast neutron recoil spectroscopy with a 4he scintillation detector," *Nuclear Instruments and Methods in Physics Research Section A: Accelerators, Spectrometers, Detectors and Associated Equipment*, vol. 1046, p. 167703, 2023. [Online]. Available: https://www.sciencedirect.com/science/article/pii/S0168900222009950

[17] E. V. D. van Loef, P. Dorenbos, C. W. E. van Eijk, K. Krämer, and H. U. Güdel, "High-energy-resolution scintillator: Ce3+ activated LaBr3," *Applied Physics Letters*, vol. 79, no. 10, pp. 1573–1575, 09 2001. [Online]. Available: https://doi.org/10.1063/1.1385342

[18] *CoMPASS Multiparametric DAQ Software for Physics Applications*, 2022. [Online]. Available: https://www.caen.it/products/compass/

[19] R. Brun, F. Rademakers, P. Canal, A. Naumann, O. Couet, L. Moneta, V. Vassilev, S. Linev, D. Piparo, G. GANIS, B. Bellenot, E. Guiraud, G. Amadio, wverkerke, P. Mato, TimurP, M. Tadel, wlav, E. Tejedor, J. Blomer, A. Gheata, S. Hageboeck, S. Roiser, marsupial, S. Wunsch, O. Shadura, A. Bose, CristinaCristescu, X. Valls, and R. Isemann, "root-project/root: v6.18/02," Aug. 2019. [Online]. Available: https://doi.org/10.5281/zenodo.3895860

[20] R. P. Gardner, E. Sayyed, Y. Zheng, S. Hayden, and C. W. Mayo, "Nai detector neutron activation spectra for pgnaa applications," *Applied Radiation and Isotopes*, vol. 53, no. 4, pp. 483–497, 2000. [Online]. Available: https://www.sciencedirect.com/science/article/pii/S0969804300001986

[21] J. Kiener, V. Tatischeff, I. Deloncle, N. de Séréville, P. Laurent, C. Blondel, M. Chabot, R. Chipaux, A. Coc, S. Dubos, A. Gostojic', N. Goutev, C. Hamadache, F. Hammache, B. Horeau, O. Limousin, S. Ouichaoui, G. Prévot, R. Rodríguez-Gasén, and M. Yavahchova, "Fast-neutron induced background in labr3:ce detectors," *Nuclear Instruments and Methods in Physics Research Section A: Accelerators, Spectrometers, Detectors and Associated Equipment*, vol. 798, pp. 152–161, 2015. [Online]. Available: https://www.sciencedirect.com/science/article/pii/S0168900215008517

[22] M. E. Rising, J. C. Armstrong, S. R. Bolding, F. B. Brown, J. S. Bull, T. P. Burke, A. R. Clark, D. A. Dixon, R. A. Forster, III, J. F. Giron, T. S. Grieve, H. G. Hughes, III, C. J. Josey, J. A. Kulesza, R. L. Martz, A. P. McCartney, G. W. McKinney, S. W. Mosher, E. J. Pearson, C. J. Solomon, Jr., S. Swaminarayan, J. E. Sweezy, S. C. Wilson, and A. J. Zukaitis, "MCNP® Code Version 6.3.0 Release Notes," Los Alamos National Laboratory, Los Alamos, NM, USA, Tech. Rep. LA-UR-22-33103, Rev. 1, January 2023. [Online]. Available: https://www.osti.gov/biblio/1909545

[23] S. Usman and A. Patil, "Radiation detector deadtime and pile up: A review of the status of science," *Nuclear Engineering and Technology*, vol. 50, no. 7, pp. 1006–1016, 2018. [Online]. Available: https://www.sciencedirect.com/science/article/pii/S1738573318302596

[24] B. Pehlivanovic, S. Avdic, P. Marinkovic, S. Pozzi, and M. Flaska, "Comparison of unfolding approaches for monoenergetic and continuous fast-neutron energy spectra," *Radiation Measurements*, vol. 49, pp. 109–114, 2013. [Online]. Available: https://www.sciencedirect.com/science/article/pii/S1350448712003575

[25] M. Febbraro, B. Becker, R. deBoer, K. Brandenburg, C. Brune, K. Chipps, T. Danley, A. D. Fulvio, Y. Jones-Alberty, K. Macon, Z. Meisel, T. Massey, R. Newby, S. Pain, S. Paneru, S. Shahina, M. Smith, D. Soltesz, S. Subedi, I. Sultana, and R. Toomey, "Performance of neutron spectrum unfolding using deuterated liquid scintillator," *Nuclear Instruments and Methods in Physics Research Section A: Accelerators, Spectrometers, Detectors and Associated Equipment*, vol. 989, p. 164824, 2021. [Online]. Available: https://www.sciencedirect.com/science/article/pii/S0168900220312213

[26] S. Agostinelli, J. Allison, K. Amako, J. Apostolakis, H. Araujo, P. Arce, M. Asai, D. Axen, S. Banerjee, G. Barrand, F. Behner, L. Bellagamba, J. Boudreau, L. Broglia, A. Brunengo, H. Burkhardt, S. Chauvie, J. Chuma, R. Chytracek, G. Cooperman, G. Cosmo, P. Degtyarenko, A. Dell'Acqua, G. Depaola, D. Dietrich, R. Enami, A. Feliciello, C. Ferguson, H. Fesefeldt, G. Folger, F. Foppiano, A. Forti, S. Garelli, S. Giani, R. Giannitrapani, D. Gibin, J. Gómez Cadenas, I. González, G. Gracia Abril, G. Greeniaus, W. Greiner, V. Grichine, A. Grossheim, S. Guatelli, P. Gumplinger, R. Hamatsu, K. Hashimoto, H. Hasui, A. Heikkinen, A. Howard, V. Ivanchenko, A. Johnson, F. Jones, J. Kallenbach, N. Kanaya, M. Kawabata, Y. Kawabata, M. Kawaguti, S. Kelner, P. Kent, A. Kimura, T. Kodama, R. Kokoulin, M. Kossov, H. Kurashige, E. Lamanna, T. Lampén, V. Lara, V. Lefebure, F. Lei, M. Liendl, W. Lockman, F. Longo, S. Magni, M. Maire, E. Medernach, K. Minamimoto, P. Mora de Freitas, Y. Morita, K. Murakami, M. Nagamatu, R. Nartallo, P. Nieminen, T. Nishimura, K. Ohtsubo, M. Okamura, S. O'Neale, Y. Oohata, K. Paech, J. Perl, A. Pfeiffer, M. Pia, F. Ranjard, A. Rybin, S. Sadilov, E. Di Salvo, G. Santin, T. Sasaki, N. Savvas, Y. Sawada, S. Scherer, S. Sei, V. Sirotenko, D. Smith, N. Starkov, H. Stoecker, J. Sulkimo, M. Takahata, S. Tanaka, E. Tcherniaev, E. Safai Tehrani, M. Tropeano, P. Truscott, H. Uno, L. Urban, P. Urban, M. Verderi, A. Walkden, W. Wander, H. Weber, J. Wellisch, T. Wenaus, D. Williams, D. Wright, T. Yamada, H. Yoshida, and D. Zschiesche, "Geant4—a simulation toolkit," *Nuclear Instruments and Methods in Physics Research Section A: Accelerators, Spectrometers, Detectors and Associated Equipment*, vol. 506, no. 3, pp. 250–303, 2003. [Online]. Available: https://www.sciencedirect.com/science/article/pii/S0168900203013688

[27] J. Allison, K. Amako, J. Apostolakis, H. Araujo, P. Arce Dubois, M. Asai, G. Barrand, R. Capra, S. Chauvie, R. Chytracek, G. Cirrone, G. Cooperman, G. Cosmo, G. Cuttone, G. Daquino, M. Donszelmann, M. Dressel, G. Folger, F. Foppiano, J. Generowicz, V. Grichine, S. Guatelli, P. Gumplinger, A. Heikkinen, I. Hrivnacova, A. Howard, S. Incerti, V. Ivanchenko, T. Johnson, F. Jones, T. Koi, R. Kokoulin, M. Kossov, H. Kurashige, V. Lara, S. Larsson, F. Lei, O. Link, F. Longo, M. Maire, A. Mantero, B. Mascialino, I. McLaren, P. Mendez Lorenzo, K. Minamimoto, K. Murakami, P. Nieminen, L. Pandola, S. Parlati, L. Peralta, J. Perl, A. Pfeiffer, M. Pia, A. Ribon, P. Rodrigues, G. Russo, S. Sadilov, G. Santin, T. Sasaki, D. Smith, N. Starkov, S. Tanaka, E. Tcherniaev, B. Tome, A. Trindade, P. Truscott, L. Urban, M. Verderi, A. Walkden, J. Wellisch, D. Williams, D. Wright, and H. Yoshida, "Geant4 developments and applications," *IEEE Transactions on Nuclear Science*, vol. 53, no. 1, pp. 270–278, 2006.

[28] J. Allison, K. Amako, J. Apostolakis, P. Arce, M. Asai, T. Aso, E. Bagli, A. Bagulya,

S. Banerjee, G. Barrand, B. Beck, A. Bogdanov, D. Brandt, J. Brown, H. Burkhardt, P. Canal, D. Cano-Ott, S. Chauvie, K. Cho, G. Cirrone, G. Cooperman, M. Cortés-Giraldo, G. Cosmo, G. Cuttone, G. Depaola, L. Desorgher, X. Dong, A. Dotti, V. Elvira, G. Folger, Z. Francis, A. Galoyan, L. Garnier, M. Gayer, K. Genser, V. Grichine, S. Guatelli, P. Guèye, P. Gumplinger, A. Howard, I. Hřivnáčová, S. Hwang, S. Incerti, A. Ivanchenko, V. Ivanchenko, F. Jones, S. Jun, P. Kaitaniemi, N. Karakatsanis, M. Karamitros, M. Kelsey, A. Kimura, T. Koi, H. Kurashige, A. Lechner, S. Lee, F. Longo, M. Maire, D. Mancusi, A. Mantero, E. Mendoza, B. Morgan, K. Murakami, T. Nikitina, L. Pandola, P. Paprocki, J. Perl, I. Petrović, M. Pia, W. Pokorski, J. Quesada, M. Raine, M. Reis, A. Ribon, A. Ristić Fira, F. Romano, G. Russo, G. Santin, T. Sasaki, D. Sawkey, J. Shin, I. Strakovsky, A. Taborda, S. Tanaka, B. Tomé, T. Toshito, H. Tran, P. Truscott, L. Urban, V. Uzhinsky, J. Verbeke, M. Verderi, B. Wendt, H. Wenzel, D. Wright, D. Wright, T. Yamashita, J. Yarba, and H. Yoshida, "Recent developments in geant4," *Nuclear Instruments and Methods in Physics Research Section A: Accelerators, Spectrometers, Detectors and Associated Equipment*, vol. 835, pp. 186–225, 2016. [Online]. Available: https://www.sciencedirect.com/science/article/pii/S0168900216306957

[29] C. C. Lawrence, A. Enqvist, M. Flaska, S. A. Pozzi, A. Howard, J. Kolata, and F. Becchetti, "Response characterization for an ej315 deuterated organic-liquid scintillation detector for neutron spectroscopy," *Nuclear Instruments and Methods in Physics Research Section A: Accelerators, Spectrometers, Detectors and Associated Equipment*, vol. 727, pp. 21–28, 2013. [Online]. Available: https://www.sciencedirect.com/science/article/pii/S0168900213007948